A highly sensitive ultrathin-film iron corrosion sensor encapsulated by an anion exchange membrane embedded in mortar

CrossMark

Healin Im [a], Yunsu Lee [b], Do Hyeong Kim [a], Omkaram Inturu [a], Na Liu [a], Sungho Lee [c], Seung-Jun Kwon [d], Han-Seung Lee [b,*], Sunkook Kim [a,*]

[a] School of Advanced Materials Science & Engineering, Sungkyunkwan University, 16419, Republic of Korea
[b] Dept. of Architectural Engineering, Hanyang University, Sangnok-gu, Ansan, Gyeonggi-do, Republic of Korea
[c] Korea Electronics Technology Institute, Gyeonggi 13488, Republic of Korea
[d] Dept. of Civil and Environmental Engineering, Hannam University, Daejeon 306-791, Republic of Korea

HIGHLIGHTS

- Embedding sensors in a fresh mortar.
- Chlorides permeating toward anion exchange membrane of sensors.
- Corroding iron channel by diffused chlorides.
- Occurring rapid variation in electrical changes of sensors by diffused chlorides.
- Indicating corrosion velocities at the spot based on the surrounding condition.

ARTICLE INFO

ABSTRACT

In this paper, an embedded ultrathin-film iron (Fe) corrosion sensor passivated with an anion-exchange membrane is developed to reveal the extent of corrosion tendency in reinforced concrete. Rebar in reinforced concrete is mainly corroded due to penetration of chloride ions which are one of the most dominant degradation factor for reinforced concrete. An effective method to monitor the extent of corrosion is to determine the positions where the chloride ions are present beyond the chloride threshold level (CTL). The sensors consist of ultrathin-film iron (Fe) layers deposited on the PET substrate, Au lines as electrode connection lines, and anion exchange membrane encasing the sensor. As the chloride ions exist near Fe layer of sensors, as if rebar has been corroded in reinforced concrete, the macro cells which occur relatively low anode and high cathode with somehow distance between them are made up and pitting corrosion accelerates. The pitting corrosion on the Fe layer of sensor induces the variation of electrical properties, which indicates the corrosion level using variations of resistance (R) and electrical response (R/R_0). To protect the sensor from mechanical and chemical stimuli in a concrete, sensors are encapsulated with an anion exchange membrane that functions not only as a protector, but also as a selector of anions including chloride ions among degradation factors. Therefore, by embedding sensors at every 10 mm depth from the surface of reinforced concrete, we can monitor the corrosion tendency causing penetration of chloride ions with respect to depth. Through the variation of electrical properties in sensors, the velocity of corrosion ($\Delta R \cdot R_0^{-1} \cdot t^{-1}$) is suggested as a new parameter, which shows the tendency for corrosion under the surrounding conditions. To confirm the relationship between corrosion velocity as determined by the sensor and the concentration of diffused chloride ions, the chloride concentration in mortar is measured. The developed sensors in this paper are effective to sensitively and accurately monitor the corrosion level of concrete.

© 2017 Elsevier Ltd. All rights reserved.

1. Introduction

Reinforced concrete has been applied toward improving the durability of structures and buildings. As the reinforcement material possesses a high tensile strength, the concrete provides a

* Corresponding authors.
    E-mail addresses: ercleehs@hanyang.ac.kr (H.-S. Lee), seonkuk@skku.edu (S. Kim).

higher stability to compression and tensile stresses. Due to this stability to external stresses, reinforced concrete is widely used as a framework for buildings, bridges, and massive structures. While rebar presents concrete with high structural stability, it can cause several problems, such as delamination and pitting corrosion [1,2]. Therefore, to monitor degradation factors for rebar are essential and indispensable.

The chemical property of reinforced concrete involves a strong alkaline environment with pH values as high as 12.5; rebar is surrounded with an oxide layer that creates a neutral shell to prevent rebar corrosion [2,3]. As time passes, the diffusion of degradation factors can change the environment of the reinforced concrete [4]. Chloride ions are largely proportional and the most dominant factors among the degradation factors affecting the induction of pitting corrosion on the surface of rebar within concrete [2,4,5]. Although the alkaline environment remains within concrete, corrosion can occur due to the diffusion of chloride ions into concrete. If diffused chloride ions exceed the chloride threshold level (CTL), the local part of the oxide layer can begin to be eroded. Due to the difference in electrical potential, electrochemical cells are produced on the rebar surface, initiating pitting corrosion [3,5–7]. Pitting corrosion of rebar is a major factor reducing the strength and life-time of reinforced concrete. Therefore, it is necessary to monitor the diffusion behavior of chloride ions that can initiate corrosion of rebar within reinforced concrete [8].

In the field, chloride monitoring is largely divided into two methods: destructive monitoring and the non-destructive monitoring [9]. Destructive monitoring is destroys specimens and directly analyzes their components within the pore solutions of reinforced concrete. However, the destructive method can overestimate or underestimate the amount of chloride ions extracted within the pore solution, these errors can result in inefficient and inaccurate monitoring results. To overcome these limitations, non-destructive monitoring systems have been developed [5–7]. In the case of non-destructive monitoring, sensors are directly embedded within the concrete and the possibility for error is relatively reduced. Several electrochemical techniques are used in non-destructive monitoring, such as potentiometric measurements with embedded electrodes, a chronopotentiometric approach [3,10] with embedded electrodes, and electrical resistivity and impedance measurements. Among these methods to monitor corrosion states induced by the diffusion of chloride ions, the simplest and easiest method is the electrical resistance (ER) method, consisting of a metal component as a reactive channel to corrosion, which has been chosen and widely studied [11–13]. ER sensors are relatively simple compared to other electrochemical methods and are easy to fabricate with a highly competitive price. Besides, ER sensors can be directly embedded and used to detect the penetration of chloride ions within reinforced concrete, showing the variation in metal mass and resistance. The resistance of the metal within the sensors can indicate certain properties, such as the intrinsic resistivity, geometry, mass, and corrosion velocity. As the magnitude of the metal resistance increases, the mass of the metal decreases [12–15]. However, ER sensors also possess several limitations, including low sensitivity and unreliability [12]. The sensitivity of ER sensors can be related to the thickness of the metal used as the sensor channel. If the metal thickness increases, the life-time of the sensor increases, at the same time, the response time will increase as well [11,16]. Therefore, it is complicated to produce sensors that satisfy both an adequately high life-time with a high sensitivity to corrosion spontaneously.

To overcome the limitations of the prior corrosion sensors, ion exchange membranes (IEMs) are a possible candidate; herein, a novel integration between IEMs and corrosion sensors is attempted. IEMs are semi-permeable membranes that filter specific charged molecules [17,18]. Numerous applications exist including electro-dialysis, the production of acids and bases, desalination of sea water, removal of heavy metals from industrial waste water, and the collection of organic acids and amino acids within the fermentation industry [17–22]. The charged ion selectivity of IEMs corresponds to the existence of functional groups with specific charged ions on the membrane surface. The specific charge of the membrane interacts electrically with mobile ions in the solution [17,22]. If the membrane is positively charged by functional groups on the surface, a repulsive force emerges with positively charged mobile molecules, and an attractive force is created with negatively charged molecules. Molecules that are attracted to the membranes can permeate through the membrane; repetition of this process results in the separation of molecules in the solution by the IEM. Depending on the surface charge of the IEMs, they can fall into the category of either anion exchange membranes (AEM) or cation exchange membranes (CEM). These membranes can be selectively used according to their application.

In this paper, we demonstrate an ultrathin-film iron (Fe) sensor surrounded with an AEM to achieve a highly reactive and stable sensor to monitor extents of corrosion. Compared to prior studies, the sensors exhibited high corrosion reactivity through an ultrathin Fe layer with a thickness of 500 nm and improved mechanical and chemical stability through encapsulating AEM. As chloride ions existed near the Fe layers within sensor, if the rebar was corroded within the reinforced concrete, pitting corrosion occurred and accelerated, causing the electrical properties of the sensors to change. The sensors can monitor the corrosion levels within mortar, by measuring the variation in electrical resistance (R) and response (R/R_0) of the sensor. Through variation in electrical properties, a corrosion velocity ($\Delta R \cdot R_0^{-1} \cdot t^{-1}$) term was defined, which was a novel parameter used to indicate the extent of corrosion regardless of experiment circumstances. Additionally, to confirm the relationship between corrosion velocities determined by the sensor and the concentration of diffused chloride ions, the chloride concentration within mortar was measured through destructive methods. The rest of the paper is classified as followings: Section 2 describes the experimental setup including materials, analysis tools, the fabrications of sensors, the preparation of mortar specimens, and the chloride penetration profile. Section 3 discusses the experimental results and Section 4 presents the conclusion.

2. Experimental setup

2.1. Anion exchange membrane (AEM)

The AEM was composed of a strong base on a polypropylene-based heterogeneous membrane with the Cl ion form. Its thickness was 0.03175–0.03429 cm in the dry status. The AEM was chemically stable between a pH of 0–14 and could avoid osmotic shock in an 8% NaOH solution.

2.2. Analysis of the AEM

The AEM was analyzed via scanning electron microscopy (SEM) and Fourier transform infrared spectroscopy (FT-IR). SEM analysis proceeded via 10.00 kV EHT at 1.50 K magnification and FT-IR spectroscopy (Spectrum One System, Perkin-Elmer) yielded a resolution better than 0.5 cm^{-1} for absorptions between the frequency range of 4500–400 cm^{-1} and in the surrounding air.

2.3. Fabrication of the sensors

The entire structure of the sensor can be seen in Fig. 1. The entire fabrication process can be largely divided into three parts: preparation of the sensor, preparation of the electrode connection lines, and
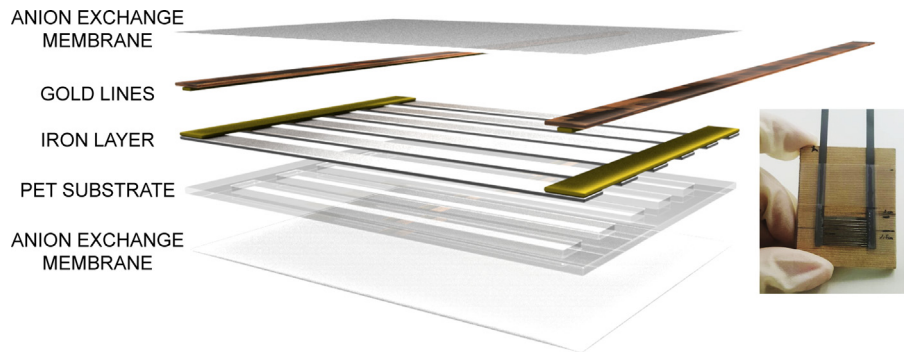
Fig. 1. Structure of ultrathin-film iron (Fe) sensor. (Inset: the photograph of ultrathin-film Fe sensor unwrapped by anion exchange membrane (AEM)).

wrapping sensor and lines in the anion exchange membrane. With regard to the sensor preparation, pre-cut and a ladder-like patterned Polyethylene terephthalate (PET) film consisted of 6 horizontal lines and 2 vertical lines used as the substrate. The entire substrate was 20 mm and 14 mm in the horizontal and vertical directions, respectively. The width of the horizontal line was 1.5 mm and the gap between lines was 1 mm. The width and length of a vertical line were 1.5 mm, respectively. After patterning of the substrate, metals were deposited in two steps; active matrix deposition and electrode deposition. The first active matrix deposition step was an iron (Fe) deposition. Fe, which was used to sense corrosion as an active matrix, was deposited by an electron-beam evaporator. Fe is deposited in the form of a 500 nm ultrathin-film onto the substrate which afforded high sensitivity to monitor chloride. Prior to the second deposition, a shadow mask was used to prevent titanium (Ti) and gold (Au) from being deposited onto the channels of the corrosion sensor. The second deposition step involved the Ti and Au depositions. Ti was used as an adhesion layer between Fe and Au due to the lack of adhesion between them, and Au was used as a contact pad for anisotropic conductive film (ACF) bonding. Ti and Au were deposited onto two vertical lines of the substrate, with thicknesses of 10 nm and 100 nm, respectively.

With regard to preparation of the electrode connection lines, a solution of polyimide (PI) was spin-coated onto glass, soft-baked at 90 °C for 5 min, and baked in an oven for over 6 h. The PI film deposited with 10 nm Ti and 100 nm Au was removed from the glass and cut to an appropriate size. The line width was 1.5 mm, and the film length was up to 80 mm. The contact pads of the sensor and electrode connection lines were integrated through ACF bonding. The electrode connection lines were sealed with another film to protect from physical stress during the concrete embedding process. Prior to wrapping, the AEM was cut to 30 mm in each direction. The AEM enclosed the sensor side of attachment except for the electrode connection lines in order to prevent the Fe layer from peeling off of the PET due to weak adhesion between the ultrathin Fe layer and the PET substrate in highly alkaline solutions.

2.4. Solution preparation and the solution test method

$[Cl^-]/[OH^-]$ was chosen as a representation of the CTL in this study and indicated that chloride ions and hydroxyl ions were factors affecting corrosion and corrosion inhibition, respectively. In order to adjust the solution condition to be as close as possible to the concrete environment [23], $Ca(OH)_2$ was added. Table 1 shows the solution composition of the test solution. The hydroxyl ion was fixed to 0.046 M and the amount of NaCl (s) was adjusted to prepare various $[Cl^-]/[OH^-]$ ratios from 0.15 to 0.90 in solution.

The solution test was considered to be an accelerated experiment because the solution conditions were more severe to induce

Table 1
Composition of the pH 12 solution.

$[Cl^-]/[OH^-]$	D.I. water (mL)	$Ca(OH)_2$ (g)	NaCl (g)
0.00	100	0.34	0.00
0.15	100	0.34	0.04
0.30	100	0.34	0.08
0.45	100	0.34	0.12
0.60	100	0.34	0.16
0.75	100	0.34	0.20
0.90	100	0.34	0.24

corrosion on the ultrathin Fe layer compared to normal concrete conditions. To investigate the sensor responses to corrosion, each sensor was directly exposed to measure the electrical response (R/R_0) and corrosion velocity ($\Delta R \cdot R_0^{-1} \cdot t^{-1}$).

In this research, the solution test proceeded by three methods. First, the sensor enclosed by the AEM was exposed to distilled water to determine its life-time and stability. Second, to confirm the functions of the AEM, sensors with and without an AEM were immersed into various solutions; this was referred to as the AEM effect test. Finally, to quantify the corrosion behaviors of the sensors, each sensor encased with an AEM was immersed within a solution with a certain ratio of chloride to hydroxyl ions. Then, the electrical resistance of the sensors was measured every 1 h within the solution, without exposure to air. The electrical resistance was directly measured from the electrode connection lines.

2.5. Mortar specimen preparation and the mortar immersion test in solution

Table 2 shows the material quantities and ratios for mortar preparation based on ASTM C109/C109 M. Ordinary Portland Cement (OPC) was used as the cement, with distilled water. In addition, the sensors were embedded within the specimen, which didn't affect the strength of the mortar [13]. The preparation process for the mortar and mortar test can be described as follows:

(1) Cement, sand, and water are mixed together.
(2) The mix, which is called mortar, is poured into a mold with sensors. The mold is used as a formwork for casting of the mortar. As shown in Figs. 2 and 3, the mold possesses 3 sec-

Table 2
Mix proportion of the mortar.

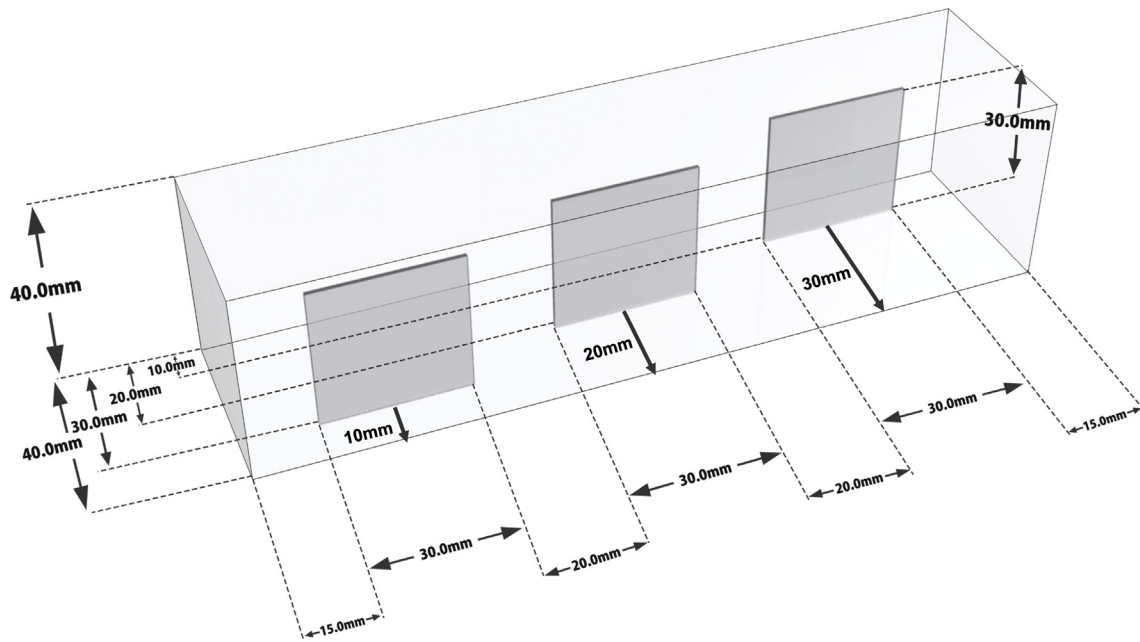| Water to Cement Ratio	Sand to Cement Ratio	The mass of materials		
		Water (g)	Cement (g)	Sand (g)
0.485	2.75	514	1060	2915

Fig. 2. Design of mold structure of mortar specimen.

Fig. 3. Photo of mold structures of mortar specimen.

tions where sensors are attached and its size is 40 mm × 40 mm × 160 mm. The closest section from the surface is located 10 mm from the surface and the interval between sections is 10 mm.

(3) The mortar is held at room temperature for 24 h.
(4) All mortar specimens are cured within a humidity chamber at 20 °C under RH 60% for 5 days.
(5) The specimens are coated with epoxy except the surface in the direction of chloride ion penetration, as can be seen in Fig. 4.
(6) The specimen is immersed in a solution with a chloride ion concentration of 1.9 wt%.

(7) The electrical resistance of the embedding sensors in the solution is measured every day and is never removed from the water. The electrical resistance is directly measured from the Au line.

2.6. Chloride penetration profile in the mortar specimen

In order to accurately predict corrosion within the mortar, it was necessary to confirm and understand the chloride profile within the mortar. The chloride content within the mortar could be measured directly although destructive methods at each depth. To obtain the standard chloride profile in this work, we analyzed the chloride profiles of the mortar whose mixture proportions are shown in Table 2. The size of the mortar was 50 mm × 50 mm × 50 mm. The mortar surfaces were coated with an epoxy resin, excluding the surface in the direction of diffusion. The mortar specimens were separated into 3 groups: initial condition, 14-day exposure and 42-day exposure. The initial condition group was to confirm the initial chloride content without immersion or chloride diffusion in the mortar. The other groups represented mortars that were immersed in a chloride solution and remained immersed for the specific exposure period. After the exposure period, the mortars were removed from the solution. Mortar specimens for both groups were cut at 7 mm intervals, and the pieces were pulverized and passed through 850 μm (No. 20) sieved. Then, the chloride content was analyzed via a silver nitrate potentiometric titration method in accordance with ASTM C1218. Based on the results, the diffused chloride content could be obtained and compared with the results for each group at every depth.

3. Results and discussions

3.1. SEM/FT-IR analysis of the AEM

Fig. 5 shows SEM images of the AEM; Fig. 5(a) is a top-view and 5(b) is a side view. The AEM was heterogeneous and contained many uneven open pores with diameters of approximately 10–40 μm. Close inspection of the pores on the surface of the AEM showed that they were randomly arranged at the micro scale.
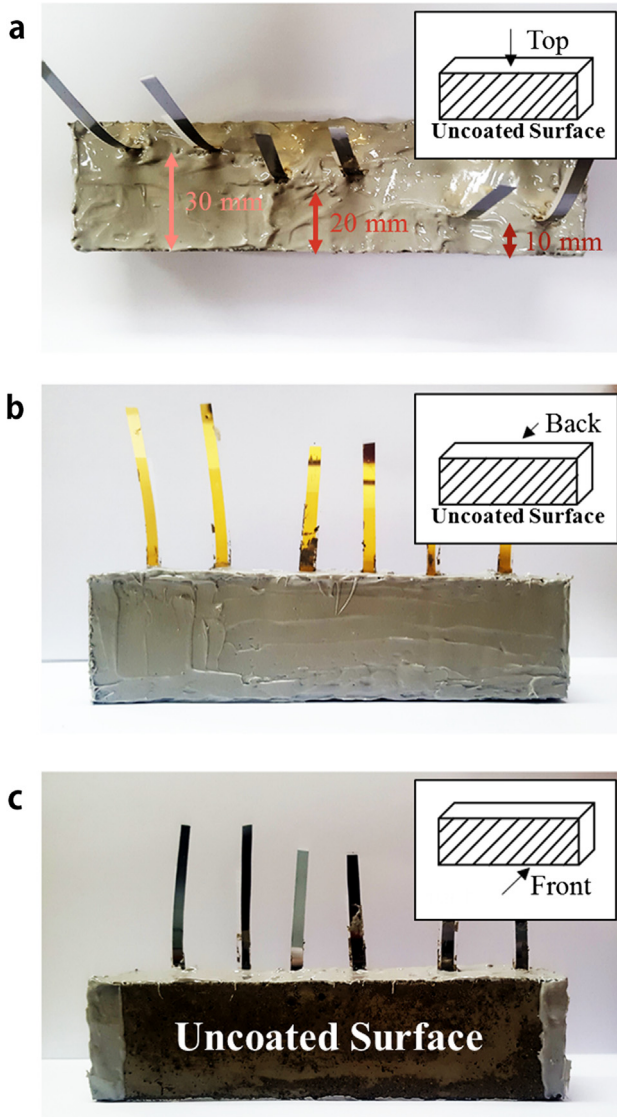
Fig. 4. Epoxy-coated mortar specimen. (a) top side (b) back side (c) front side.
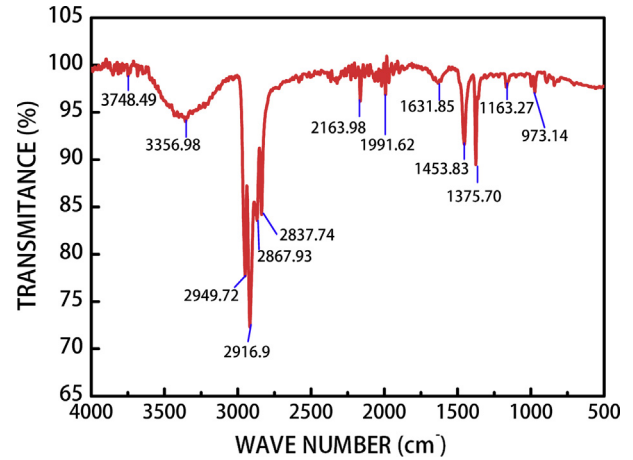

Fig. 6. FT-IR analysis of AEM.

to 3550 cm^{-1}. The presence of a characteristic signal for the hydroxide anion (O—H stretching at approximately 3500 cm^{-1}) indicated complete ion exchange. Alkanes have three major peaks for C=C bonds, which are symmetric and show reduced intensity and stretch asymmetry of peaks, compared to =C—H and =CH$_2$ bonds, whose peaks are intense. In this case, the infrared spectra results of the AEM exhibited a typical broad C—H alkyl stretching band from 2850 cm^{-1} to 3000 cm^{-1}. Peaks at 2949, 2916, 2867, and 2837 cm^{-1} could be assigned to the C—H band, while the band at 2950 cm^{-1} could be attributed to saturated hydrocarbon. The reflected C≡C bond absorption peaks in the wavelength range from 2000 cm^{-1} to 2400 cm^{-1} could be attributed to instrument error caused by the diamond mirror of the FT-IR spectrum analysis equipment. The peak at 1450 cm^{-1} was assigned to CH$_2$ bonds, and —CH$_3$— bands were shown between the range of the 1450–1370 cm^{-1}. The C—H band has out of plane bending (oop) absorption at 1000–650 cm^{-1}; the presence of 1,2-disubstituted (*trans*) groups produced a band near 970 cm^{-1}, and the 1,1-disubstituted groups produced a strong band near 890 cm^{-1}.

3.2. Solution test

3.2.1. Stability test

Fig. 7 shows the stability of the thin-film Fe sensor encapsulated by the anion exchange membrane in distilled water to confirm the stability of the sensor. The AEM encased thin-film Fe sensor was immersed in the solution at room temperature. The initial electrical resistance of the Fe sensor was 50 ohms as shown in the inset of Fig. 7; the value was then measured once a day for 25 days. In order to generalize the change of electrical resistance, the electrical response (R/R_0) was obtained by an increase in resistances and electrical response from 1 to 1.2.
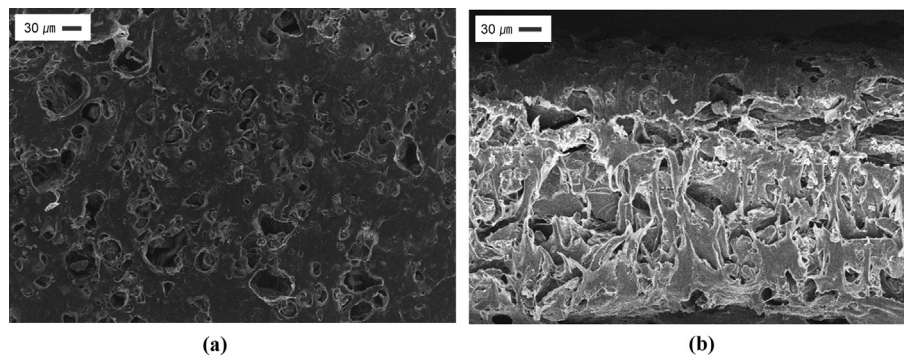
The side-view of the AEM in Fig. 5(b) shows irregular paths created by overlapping pores penetrating through the membrane. The diameter of the irregular paths was less than 30 μm. Fig. 6 shows the FT-IR spectra of the AEM. With regard to alcohols and phenols, free O—H groups usually appear as sharp peaks from 3580 cm^{-1} to 3650 cm^{-1}, broad absorption peaks are consistent with the characteristic N—H or O—H stretching vibrational bands from 3200 cm^{-1}
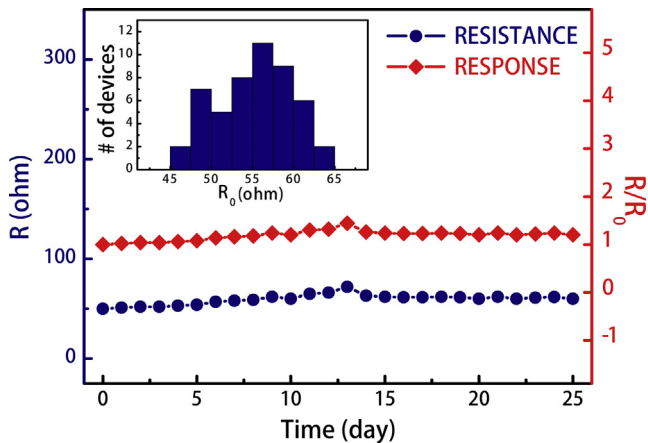

Fig. 5. SEM image of AEM; (a) top-view (b) side-view.

Fig. 7. Stability of ultrathin film Fe sensor encased with AEM in distilled water. (Inset: distribution of initial resistances.)

Fig. 8. Electrical response of sensors with respect to $[Cl^-]/[OH^-]$ after 7 days immersing.

As shown in Fig. 7, the resistance and response increased slightly. Although there were no chloride ions, a natural electrical potential difference occurred at the surface of the Fe layer in the solution condition [2,6,16]. The potential difference at the surface of the Fe layer induced corrosion of the Fe layer and generated ferric oxide (Fe_2O_3) as a product of corrosion on the Fe channel surface. Due to the production of ferric oxide, the electrical resistance increased, the mass of metal decreased, and the charge on the surface of the AEM corroded the Fe layer. Therefore, the electrical resistance and response increased slightly.

The electrical resistance and response from 12 to 14 days were scattered due to variations in measurements through two different contact resistance; contact between an electrode of the sensor and the electrode connection lines, and contact between the Au line and the measurement equipment. Although this study used ACF bonding to stabilize the contact resistance without variation, variation still occurred due to contact resistance between the electrodes and the measuring equipment. Although there was a lifetime limitation due to a thin Fe layer [16], the sensor enabled similar maintenance of the resistance and response. Therefore, the lifetime of the sensor was maintained without dramatic reduction in the reactivity of the sensor [12].

3.2.2. AEM effect test

The AEM effect was investigated by using encased and exposed sensors. Fig. 8 shows the electrical response (R/R_0) of both sensors with respect to $[Cl^-]/[OH^-]$ after immersion for 7 days in a pH 7 solution. As the thin-film Fe layer peeled off the PET substrate without an AEM in a pH 13 solution, the two types of sensors could not be compared at pH 13 and were instead compared at pH 7. In Fig. 8, the orange and green lines represent the electrical responses of the exposed and encased types after immersion for 7 days, respectively. The response of both sensors in distilled water was almost similar, indicating no effect of the AEM in distilled water. However, depending on the existence of the AEM, the response differed as a function of the extent of chloride within the solution. In the case of the exposed type, despite an increased responses with an increase in $[Cl^-]/[OH^-]$, there was no linear relationship between the concentration of chloride ions and the electrical response. With an increase in $[Cl^-]/[OH^-]$, the response continued to dramatically change to 3.759, 17.857, 11.331, 15.657, 22.269, and 16.75 at $[Cl^-]/[OH^-]$ ratios of 0.15, 0.30, 0.45, 0.60, 0.75, and 0.90, respectively. Even though the highest level of salinity in the solution is 0.90, the response was lower in this solution than the response at 0.75 and was similar to the response at 0.60. However, the encased type sensor had a tendency to exhibit a quasi-linear
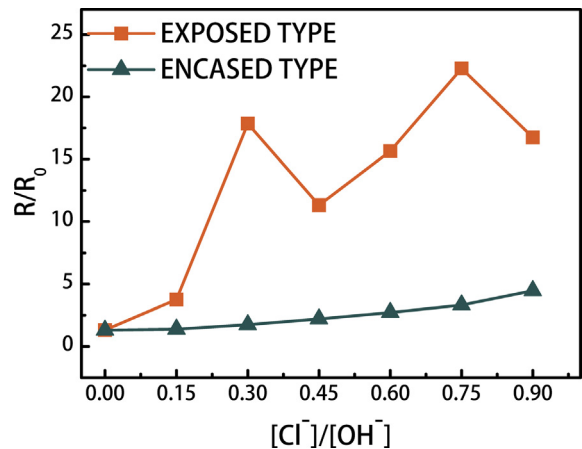
response as shown in Fig. 8. Compared to the exposed type, the change in response was initially much more stable. Despite a low response of only 4.4625 at the 0.90 ratio, it is similar to that of the exposed type at the 0.15 ratio. This indicated that the encased type had more time to corrode and showed better linearity early on.

If a sensor was exposed to a solution, numerous chloride ions in the solution rapidly approached and affected the channel Fe layer. These chloride ions induced a pitting corrosion explosively to the channel Fe layer and the critical corrosion could occur anywhere on the sensor [16]. There were several possibilities which experienced serious corrosion near junctions with the contact pads and electrode contact lines or far from the junction on the channel Fe layer. Thus, the rapid and explosive approaches of chloride ions cause poor linearity of electrical responses change. In the case of the encased type, the AEM acted as an obstacle to chloride ion penetration through the membrane to interact with the sensor channel. Most ions were interrupted by the AEM and only anions passed into the interior of the AEM [17,22] such that irregular pitting corrosion could be reduced at the surface of the Fe layer. The AEM induced a positive effect to enhance the linearity between the change in response and $[Cl^-]/[OH^-]$.

3.2.3. Electrical response and corrosion velocity

Fig. 9 shows the solution test for monitoring the tendency of electrical response (R/R_0) of the encased type sensor with respect to $[Cl^-]/[OH^-]$ under highly alkaline conditions. The electrical resistance and response indicate the corrosion of the Fe layer in the sensor. As the AEM chemically and physically stabilized at pH 1–13, it was assumed that the conditions had no effect on changes in the AEM. Prior to immersion, the initial electrical resistance of the sensors ranged from 50 to 80 ohms as shown in inset. Before 8 h, the response in distilled water was 1.2875, and the response at 0.15 was 1.2467, which shows that the responses changed irregularly with the ratio of chloride ions to hydroxyl ions. After 8 h, the responses exhibited quasi-linear behavior with time, and the responses dramatically changed over a $[Cl^-]/[OH^-]$ of 0.6 which was known as the CTL [6,24]. In the solution with a ratio of 0.45, the response was 11.876 after being immersed for 50 h, and this response was similar to that of the response after immersion for 10 h in the 0.90 ratio solution. This was because the increased range of responses was different at specific ratios and was quantized with respect to $[Cl^-]/[OH^-]$ according to exposure time. The slopes shown in Fig. 9 saturated after initial unstable states and showed that sensors immersed in particular solution salinities tended to be corroded at certain increasing ranges after
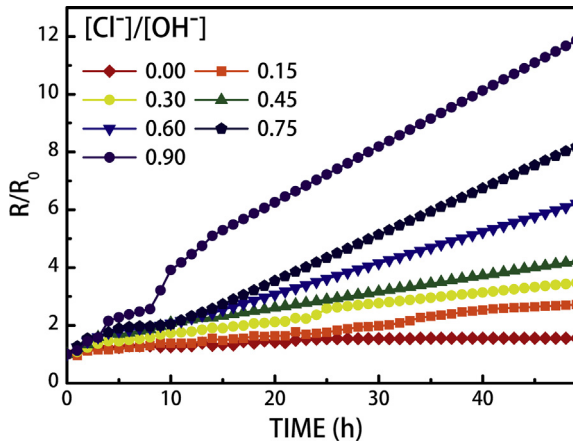
Fig. 9. Electrical response of encased type form with respect to [Cl⁻]/[OH⁻] in pH 13 solution.

Fig. 11. Electrical response with respect to depths from the surface in the mortar. (Inset: the optical image of mortar specimen.)

certain periods of time. Therefore, we defined the slope as the generalized the corrosion velocity. Eq. (1) is a function of the corrosion velocity in the solution. In this equation, the units of R and R_0 are ohms, the units of t and t_0 are hours, and t_0 is the exposing moment.

$$\text{Corrosion velocity}_{solution} = \frac{\Delta Electrical\ response}{\Delta t} = \frac{\left(\frac{R}{R_0} - \frac{R_0}{R_0}\right)}{t - t_0} = \frac{\Delta R}{R_0 \cdot t} \quad (1)$$

Using Eq. (1), the corrosion velocity was calculated as shown in Fig. 10. Each column indicated a corrosion velocity in accordance with [Cl⁻]/[OH⁻]: 0.0104, 0.0368, 0.0968, 0.1255, 0.1541, 0.1828, and 0.2255, respectively. The corrosion velocity could be used as a novel parameter to compare to the salinity in the concrete. If the embedded sensors in the concrete show a specific corrosion velocity, it could be assumed that the sensor was corroded as if it was immersed in a solution with conditions of a specific [Cl⁻]/[OH⁻] ratio with the same corrosion velocity.

3.3. Mortar immersion test

3.3.1. Electrical response and corrosion velocity

Fig. 11 shows the variation in electrical response (R/R_0) with respect to the depth from the surface where chloride ions of the
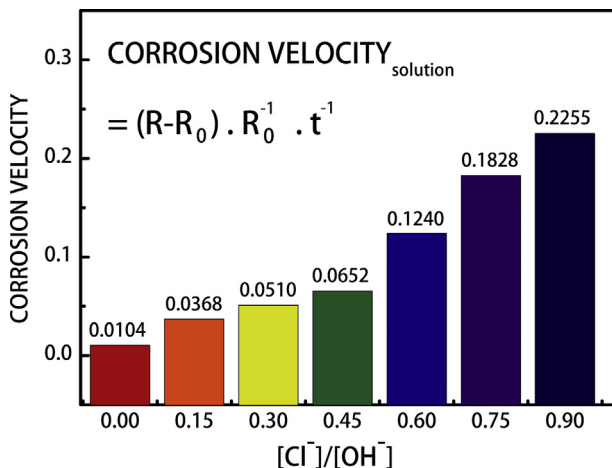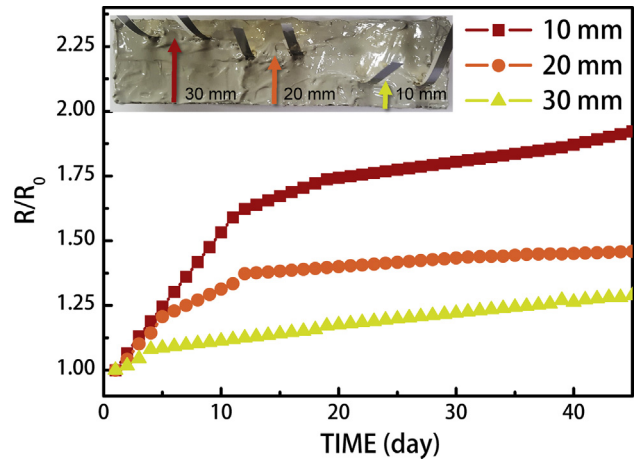
external solution penetrate through mortar. To examine experiments under the conditions experienced by structures near the sea, the external solution was adjusted to 3 wt% NaCl to simulate sea water and sensors were selected based on their resistance between a range of 50–60 ohms. The resistance of the sensors increased from 50–60 ohms to 100–120 ohms due to external stresses during the embedding process. After the sensors were embedded within the mortar, they were very stable and experienced little pitting corrosion due to the near absence of water and air within the mortar, and measurements were also performed once per day.

However, after the mortar was exposed to the solution, chloride ions diffuse toward the opposite side of the specimen perpendicular from the surface. As the diffusion of chloride ions occurred rapidly early on, the embedded sensor exhibited an increase in resistance and after sufficient time to stabilize, the increase in resistance was stabilized. The resistance of the sensors located 10 mm from the surface increased to 194 ohms and slowed down after immersion for 11 days. Additionally, the closer the sensor was located to the surface, the longer it took for the sensor to stabilize [2,4]. The increased response range from the start to 10 days was 0.59 (from 1 to 1.59) and was more than twice as large as the increased response range from 11 days to 40 days, which was 0.27. The electrical resistance of the sensor placed 20 mm from the surface became saturated at 152.5 ohms after 9 days, while the electrical resistance and response of the sensor located 30 mm from the surface increased to 120 ohms and 1.081, respectively. In short, sensors closed to the surface were more affected by the diffusion of chloride ions.

Because the diffusive behavior of chloride through mortar is difficult to investigate without destructive processes, the mortar immersion test should be compared to a condition with the known specific chloride ion diffusion. In this study, the corrosion velocity determined from the solution test was the known condition. When the corrosion velocity in the solution was defined, the condition within the solution was quite harsh to the sensors. The electrical responses of the sensors increased rapidly within a matter of hours; therefore hours were selected as the designated units for the response time. To compare the corrosion velocity in solution and through mortar, the corrosion velocity units for both experiments in mortar must be the same; the units were h⁻¹. In the mortar test, the interval between measurements was 1 day; 24 h were substituted for 1 day in Eq. (1). Therefore, the corrosion levels within mortar could be compared to the corrosion velocity in the solution.

Fig. 10. Corrosion velocity encased type form with respect to [Cl⁻]/[OH⁻] in pH 13 solution.

Fig. 12 shows the corrosion velocity with respect to the sensor depth from the surface calculated in hours. The corrosion velocities of distilled water and a 0.15 ratio solution are depicted by blue dashed lines in Fig. 12. The corrosion velocities were 0.0104 and 0.0368 in distilled water and the 0.15 solution, respectively. In the case of the sensor located 10 mm from the exposed surface, the corrosion velocity increased rapidly for 10 days prior to reaching the corrosion velocity noted in distilled water after 5 days. After 10 days, the corrosion velocity increased, although the increase was less than the increase that occur during the previous 10 days. The corrosion velocity increased gradually and reached the measured corrosion velocity in the 0.15 ratio solution after approximately 40 days. After 40 days, the sensor was dramatically corroded as if it was immersed under rapidly accelerated condition, which was over 0.15 of $[Cl^-]/[OH^-]$. The sensor located 30 mm from the surface exhibited a tendency to gradually increase after immersion and barely reached the corrosion velocity in distilled water after approximately 40 days. When the sensor located at 10 mm was corroded like it was immersed in a $[Cl^-]/[OH^-]$ ratio of 0.15, the sensor located at 30 mm began to corrode as if it were immersed in distilled water. In summary, because the corrosion behaviors due to chloride ions penetration was different depending on the depth a single specimen [4], each embedded sensors indicated a different corrosion velocity.

3.3.2. Chloride penetration profile within the mortar specimen

Fig. 13 presents the chloride penetration profile for mortar after immersion for 14 days and 42 days. Because the corrosion velocity, as shown in Fig. 12, is related to the corrosion tendency of a certain environment, it was proportional to the concentration of diffused chloride ions within the mortar, which should be a factor of the environment. To compare with the electrical result from the sensors with the real diffusion behavior of chloride ions within mortar, the concentration of chloride ions diffused through the concrete were obtained via a destructive method. The mortar under natural diffusion conditions was the same as the conditions of the mortar test. There were several factors that affected the diffusive tendency of chloride ions within the mortar: the ratio of water to cement, humidity within the mortar, and the temperature; however, the exposure time was selected as a parameter within this study. The chloride concentration was calculated from the actual chloride mass obtained within the mortar by depth. In Fig. 13, the symbols are the experiment results and the lines are fitting values. The result after 14 days of immersion is shown in green, and the result after 42 days of immersion is shown in red. The red dashed line, orange dashed line, and yellow dashed line indicate distances of
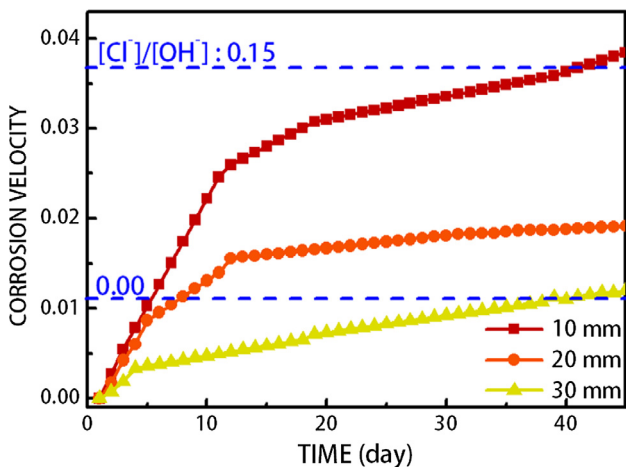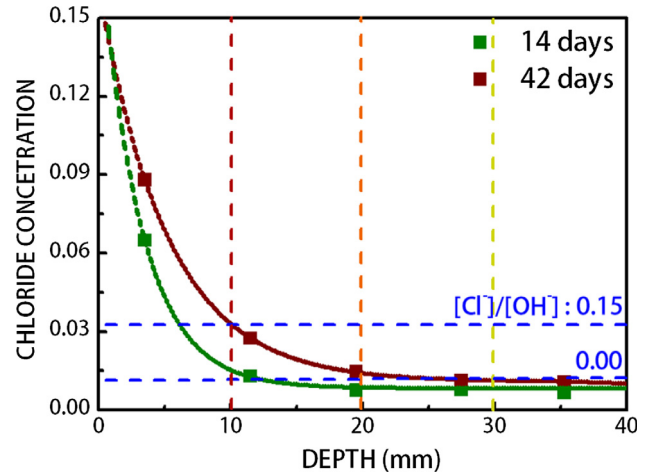

Fig. 13. Chloride penetration profile in the mortar after 14 days and 42 days.

10 mm, 20 mm, and 30 mm from the exposure surface, respectively.

Prior to immersing the specimens in solution, the initial chloride concentration in the mortar was less than 0.0069 wt% [6] in all parts. After immersing the specimens in solution, the initial chloride concentration was not maintained and chloride diffusion exhibited an exponential rate of decrease by depth. Near the surface of the mortar, the chloride concentration was approximately 0.16 wt% and was nearly unaffected by the exposure duration since there was limited chloride diffusion, which was saturated near the surface [24]. The longer the specimen was immersed in solution, the greater the amount of chloride penetrated the mortar. If the specimen was immersed in solution for 14 days, chloride ions diffused to 20 mm from the surface. The chloride concentration change at 3.5 mm was the largest variation in calculated mass and the range of increase was smaller at greater depths. The chloride concentration increased from 0.0069 wt% to 0.06488 wt% at a depth of 3.5 mm and by 0.013% and 0.007% at depths of 11.5 mm and 19.5 mm, respectively. The concentration difference between 3.5 mm and 11.5 mm was approximately 0.05%, and the difference between 11.5 mm and 19.5 mm was approximately 0.005%. After the mortar was immersed in solution for 42 days, the concentration further increased, as did the difference in the chloride concentration. The chloride concentration at 3.5 mm increased by 0.088% and was more than 12 times greater than the initial chloride concentration.

After the specimen was immersed in solution for 42 days, according to Figs. 12 and 13, the corrosion velocity at 30 mm in mortar was larger than the corrosion velocity in distilled water and the level of corrosion velocity was similar to the corrosion velocity in distilled water. It could be assumed that the corrosion tendency of the sensor in distilled water was similar to the corrosion tendency in mortar with a chloride concentration of 0.015 wt% which shows corrosion velocity at 30 mm. This chloride concentration is higher than that obtained after being immersed for 14 days at 10 mm. This provides the result that the corrosion velocity of distilled water was higher than the corrosion velocity obtained at 10 mm after immersing for 14 days. The corrosion velocity at 20 mm is greater than the corrosion velocity in distilled water but lower than 0.015 wt%. This result implied that the amount of diffused chloride ions near 20 mm was low.

From the overall results, the specific corrosion velocity could represent certain conditions within the mortar, and if the critical standard of chloride content was decided [24], the corrosion velocity at that condition could be calculated. In other words, observers could monitor the corrosion behavior from the corrosion velocity

Fig. 12. Corrosion velocity with respect to depths from the surface in the mortar.

determined through sensors embedded within certain locations of the mortar. Thus, the sensors could be a simple and effective method to non-destructively monitor chloride diffusion within mortar.

4. Conclusions

In this paper, a thin-film Fe sensor surrounded with an AEM was developed to monitor the penetration of chloride ions as a corrosion indicator for reinforced concrete. An ultrathin Fe layer of the sensor was deposited at a thickness of 500 nm and was significantly thinner than channel layers in prior studies, allowing for a highly sensitive response as a function of chloride ions. The AEM surrounded the whole channel, thereby affording a strong linear response and high stability within the mortar during embedding. When the sensor was exposed to an environment with chloride, chloride ions corroded the Fe layer, and the electrical resistance and response of the sensor increased. From these results, the corrosion velocity was newly defined and applied as a novel parameter to confirm the corrosion tendency of the condition where the sensor was imbedded. Our sensor exhibited high reactivity, reliability, and stability in mortar; observers could monitor the diffusion behavior of chloride in mortar using the corrosion velocity. Enhancements developed through this study were as follows:

(i) An ultrathin Fe layer was used as the active matrix of the corrosion sensors, enhancing their reactivity to be corrosion as compared to prior studies.
(ii) An AEM was applied for the passivation layer of sensor to protect from mechanical and chemical stresses during mortar embedment.
(iii) Through the capability for anions to permeate the AEM, the sensors exhibited high linearity as a function of $[Cl^-]/[OH^-]$ in the solution.
(iv) A newly defined corrosion velocity term was a simple and effective candidate to indicate the corrosion tendency of the surroundings including solution and mortar.

However, there are the challenges and hurdles that need to be overcame. Mortar usually consists of sand and cement roughly yet concrete also includes chippings of stones and rocks. Owing to its added elements, strength of concrete enhances relatively larger as compare to that of mortar. But there are also side effects such as a large mechanical stress, unexpected ions injection and so on. If the ultrathin Fe sensor is embedded in the concrete, the sensor should stand against much bigger mechanical stresses including irregular scratches and impacts by chippings. Also, many negative ions can make influences to the Fe channel by passing through AEM. The hurdles from differences between concrete and mortar are supposed to overcome for applying to real construction sites.

Author contributions

H. Im and Y. Lee contributed equally to this work.

Acknowledgement

References

[1] C. Arya, F.K. Ofori-Darko, Influence of crack frequency on reinforcement corrosion in concrete, Cem. Concr. Res. 26 (3) (1996) 345–353.
[2] A. Neville, Chloride attack of reinforced concrete: an overview, Mater. Struct. 28 (2) (1995) 63–70.
[3] Y. Abbas, D.B. De Graaf, W. Olthuis, A. Van den Berg, No more conventional reference electrode: transition time for determining chloride ion concentration, Anal. Chim. Acta 821 (2014) 81–88.
[4] N. Damrongwiriyanupap, L. Li, Y. Xi, Coupled diffusion of chloride and other ions in saturated concrete, Frontiers Arch. Civil Eng. China 5 (3) (2011) 267–277.
[5] C.L. Page, P. Lambert, P.R.W. Vassie, Investigations of reinforcement corrosion. 1. The pore electrolyte phase in chloride-contaminated concrete, Mater. Struct. 24 (4) (1991) 243–252.
[6] P. Lambert, C.L. Page, P.R.W. Vassie, Investigations of reinforcement corrosion. 2. Electrochemical monitoring of steel in chloride-contaminated concrete, Mater. Struct. 24 (5) (1991) 351–358.
[7] V.K. Gouda, W.Y. Halaka, Corrosion and corrosion inhibition of reinforcing steel II, Embedded Concr. British Corros. J. 5 (5) (1970) 204–208.
[8] J.P. Broomfield, K. Davies, K. Hladky, The use of permanent corrosion monitoring in new and existing reinforced concrete structures, Cem. Concr. Compos. 24 (1) (2002) 27–34.
[9] G.S. Duffó, S.B. Farina, Development of an embeddable sensor to monitor the corrosion process of new and existing reinforced concrete structures, Constr. Build. Mater. 23 (8) (2009) 2746–2751.
[10] J.M. Gandiá-Romero, I. Campos, M. Valcuende, E. García-Breijo, M.D. Marcos, J. Payá, J. Soto, Potentiometric thick-film sensors for measuring the pH of concrete, Cem. Concr. Compos. 68 (2016) 66–76.
[11] M. Raupach, P. Schießl, Macrocell sensor systems for monitoring of the corrosion risk of the reinforcement in concrete structures, NDT E Int. 34 (6) (2001) 435–442.
[12] H.S. Lee, W.J. Park, H.S. Lee, S.H. Joh, Monitoring method for the chloride ion penetration in mortar by a thin-film sensor reacting to chloride ion, Constr. Build. Mater. 53 (2014) 403–410.
[13] S. Li, S. Jung, K.w. Park, S.M. Lee, Y.G. Kim, Kinetic study on corrosion of steel in soil environments using electrical resistance sensor technique, Mater. Chem. Phys. 103 (1) (2007) 9–13.
[14] S. Jung, S. Li, Y.G. Kim, Corrosion properties of sputter-deposited steel thin film for electrical resistance sensor material, Electrochem. Commun. 8 (4) (2006) 658–664.
[15] Y.G. Kim, S. Li, S. Jung, S.M. Lee, J. Kim, Y.T. Kho, Corrosion behaviors of sputter-deposited steel thin film for electrical resistance sensor material, Surf. Coat. Technol. 201 (3–4) (2006) 1731–1738.
[16] G.S. Frankel, Pitting corrosion of metals: a review of the critical factors, J. Electrochem. Soc. 145 (6) (1998) 2186–2198.
[17] T. Xu, Ion exchange membranes: state of their development and perspective, J. Membr. Sci. 263 (1–2) (2005) 1–29.
[18] M. Higa, N. Tanaka, M. Nagase, K. Yutani, T. Kameyama, K. Takamura, Y. Kakihana, Electrodialytic properties of aromatic and aliphatic type hydrocarbon-based anion-exchange membranes with various anion-exchange groups, Polymer (United Kingdom) 55 (16) (2014) 3951–3960.
[19] S. Maurya, S.H. Shin, K.W. Sung, S.H. Moon, Anion exchange membrane prepared from simultaneous polymerization and quaternization of 4-vinyl pyridine for non-aqueous vanadium redox flow battery applications, J. Power Sources 255 (2014) 325–334.
[20] D.J. Kim, M.K. Jeong, S.Y. Nam, Research trends in ion exchange membrane processes and practical applications, Appl. Chem. Eng. 26 (1) (2015) 1–16.
[21] S.D. Poynton, J.R. Varcoe, Reduction of the monomer quantities required for the preparation of radiation-grafted alkaline anion-exchange membranes, Solid State Ionics 277 (2015) 38–43.
[22] M. Vaselbehagh, H. Karkhanechi, R. Takagi, H. Matsuyama, Surface modification of an anion exchange membrane to improve the selectivity for monovalent anions in electrodialysis – experimental verification of theoretical predictions, J. Membr. Sci. 490 (2015) 301–310.
[23] V.K. Gouda, Corrosion and corrosion inhibition of reinforcing steel I. immersed in alkaline solutions, British Corros. J. 5 (5) (1970) 198–203.
[24] D.A. Haussman, Steel corrosion in concrete. How does it occur?, J Mater. Prot. (1967) 19–23.